

A new multi-tracer pellet injection for a simultaneous study of low- and mid/high-Z impurities in high-temperature plasmas

journal or publication title	Review of Scientific Instruments
volume	92
number	6
page range	063516
year	2021-06-16
URL	http://hdl.handle.net/10655/00013570

doi: <https://doi.org/10.1063/5.0043495>



A new multi-tracer pellet injection for a simultaneous study of low- and mid/high-Z impurities in high-temperature plasmas

Cite as: Rev. Sci. Instrum. **92**, 063516 (2021); <https://doi.org/10.1063/5.0043495>
 Submitted: 08 January 2021 • Accepted: 01 June 2021 • Published Online: 16 June 2021

 N. Tamura,  M. Yoshinuma, X. Yin, et al.

COLLECTIONS

Paper published as part of the special topic on [Proceedings of the 23rd Topical Conference on High-Temperature Plasma Diagnostics](#)



View Online



Export Citation



CrossMark

ARTICLES YOU MAY BE INTERESTED IN

[Sensitivity improvement of infrared imaging video bolometer for divertor plasma measurement](#)



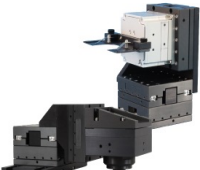
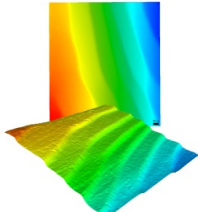
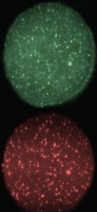
Review of Scientific Instruments **92**, 063521 (2021); <https://doi.org/10.1063/5.0043664>

[W-band millimeter-wave back-scattering system for high wavenumber turbulence measurements in LHD](#)

Review of Scientific Instruments **92**, 043536 (2021); <https://doi.org/10.1063/5.0043474>

[Measurements of radial profile of isotope density ratio using bulk charge exchange spectroscopy](#)

Review of Scientific Instruments **92**, 063509 (2021); <https://doi.org/10.1063/5.0043607>

 MCL MAD CITY LABS INC. www.madcitylabs.com	<p>Nanopositioning Systems</p> 	<p>Modular Motion Control</p> 	<p>AFM and NSOM Instruments</p> 	<p>Single Molecule Microscopes</p> 
---	--	--	---	--

A new multi-tracer pellet injection for a simultaneous study of low- and mid/high-Z impurities in high-temperature plasmas

Cite as: Rev. Sci. Instrum. 92, 063516 (2021); doi: 10.1063/5.0043495

Submitted: 8 January 2021 • Accepted: 1 June 2021 •

Published Online: 16 June 2021



View Online



Export Citation



CrossMark

N. Tamura,^{1,2,a)} M. Yoshinuma,¹ X. Yin,³ K. Ida,^{1,2} C. Suzuki,^{1,2} M. Shoji,¹ K. Mukai,^{1,2} and H. Funaba¹

AFFILIATIONS

¹National Institutes of Natural Sciences, National Institute for Fusion Science, Toki, Gifu 509-5292, Japan

²SOKENDAI (The Graduate University for Advanced Studies), Toki, Gifu 509-5292, Japan

³University of South China, Hengyang, Hunan 421001, China

Note: Paper published as part of the Special Topic on Proceedings of the 23rd Topical Conference on High-Temperature Plasma Diagnostics.

^{a)}Author to whom correspondence should be addressed: tamura.naoki@nifs.ac.jp

ABSTRACT

A new multi-tracer technique in the Tracer-Encapsulated Solid Pellet (TESPEL) method has been developed in order to acquire simultaneously the information about the behaviors of various impurities, i.e., to study concurrently the behaviors of low- and mid/high-Z impurities in magnetically confined high-temperature plasmas. In this new technique, an inorganic compound (for example, lithium titanate, Li_2TiO_3) is proposed to be used as a tracer embedded in the core of the TESPEL, instead of pure elements. The results of the proof-of-principle experiment clearly demonstrate the applicability of the new multi-tracer technique in the TESPEL method for the simultaneous study of behaviors of low- and mid/high-Z impurities in high-temperature plasmas.

Published under an exclusive license by AIP Publishing. <https://doi.org/10.1063/5.0043495>

I. INTRODUCTION

At present, challenges regarding impurities in magnetically confined fusion plasmas are becoming more complex because various impurities from low to high atomic-number (Z) elements could exist simultaneously inside the high-temperature plasma. The principle possible low- Z impurity in a fusion plasma is helium (He , $Z = 2$), which will be produced as a by-product of the deuterium–tritium (DT) fusion reaction. The major possible high- Z impurity in the same plasma would be tungsten (W , $Z = 74$), which would be used in plasma facing components. Therefore, impurity transport studies covering a variety of Z -elements are still being performed in various magnetically confined fusion experiment devices.^{1–10} In this regard, a simultaneous study of the behaviors of low- and mid/high- Z impurities would be highly important. This study will make a major contribution to a full understanding of the nature of impurity transport in the magnetically confined high-temperature plasmas. Currently, in several helical devices, such impurity transport studies are being conducted by using a

Tracer-Encapsulated Solid Pellet (TESPEL).¹¹ The TESPEL usually consists of a polystyrene $(\text{C}_8\text{H}_8)_n$ polymer as an outer layer and tracer impurities, which can be chosen from a wide range of materials, as an inner core. Until now, pure elements, such as titanium (Ti , $Z = 22$), vanadium (V , $Z = 23$), as well as many others, have been used as tracer impurities embedded in the TESPEL. In order to obtain simultaneously the behaviors of multiple impurities by using the TESPEL, the TESPEL containing triple tracers [e.g., V , manganese (Mn , $Z = 25$), and cobalt (Co , $Z = 27$)] has been developed.¹² In this multi-tracer technique, one critical point to be improved is that the gaseous elements at room temperature are not available even when needed. As a solution, we propose another new multi-tracer technique using an inorganic compound, such as an oxide and a nitride.

This paper describes the setup and results of a proof-of-principle experiment for studying simultaneously the behaviors of low- and mid/high- Z impurities in magnetically confined high-temperature plasmas with another new multi-tracer technique in the TESPEL method.

II. SETUP OF PROOF-OF-PRINCIPLE EXPERIMENT

The proof-of-principle experiment for studying simultaneously the behaviors of low- and mid/high-Z impurities in the magnetically confined high-temperature plasmas with another new multi-tracer technique in the TESPEL method has been performed in LHD. In this experiment, lithium titanate (Li_2TiO_3) was used as a tracer embedded in the core of the TESPEL. In this case, lithium (Li) and oxygen (O) are low-Z impurity tracers and titanium (Ti) is a mid-Z impurity tracer. A photo of the lithium titanate powder used here is shown in Fig. 1. As can be seen, the lithium titanate micro-powder pieces are clumped together. These lumps of lithium titanate micro-powder are formed by sintering, and the typical size of each lump is about 180–300 μm . The solidification of lithium titanate micro-powder by sintering is especially performed for easy embedding into the core of the TESPEL. The outer diameter and the inner core diameter of the TESPEL used in this experiment were 900 and ~ 300 μm , respectively.

The TESPEL containing the Li_2TiO_3 tracer (Li_2TiO_3 -TESPEL) was injected into the LHD plasmas by using the TESPEL injector (the oblique injection type),¹³ which is installed at LHD Port 3-O. This injector employs a pneumatic pipe-gun method for TESPEL acceleration, and the propellant gas (He) pressure was set at 1 MPa. In this experiment, the final guide tube position was set so that the TESPEL could reach as deeply as possible into the central region of the LHD plasma. A charge exchange spectroscopy (CXS) technique can be used to track the spatiotemporal behaviors of the fully ionized low-Z impurity tracers in the LHD. Here, since the number of target elements is more than 1, Li and O, a two-wavelength spectrometer system,¹⁴ which has been modified for this purpose, has been utilized for the measurement of CX lines of Li and O. The temporal resolution of CXS diagnostic with the modified two-wavelength spectrometer is 20 ms. In the proof-of-principle experiment, a simultaneous observation of Li III ($n = 5 \rightarrow 4$, $\lambda = 449.9$ nm) and O VIII ($n = 10 \rightarrow 9$, $\lambda = 606.9$ nm) spectral lines is attempted. In order to observe line emissions from the highly charged Ti ions, a VUV/EUV spectrometer, SOXMOS,¹⁵ which is installed at Port 7-O, is used. SOXMOS has just a single sightline, which is along the major radius at the horizontally elongated poloidal cross section of LHD. The typical temporal resolution of SOXMOS is 50 ms. The spatiotemporal evolution of the electron density and temperature is measured

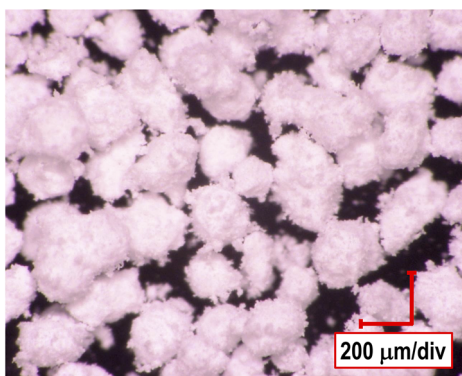


FIG. 1. Photograph of lithium titanate (Li_2TiO_3) powder used for the proof-of-principle experiment.

with a Thomson scattering diagnostic.¹⁶ The typical temporal resolution of the Thomson scattering diagnostic is 33 ms. Finally, the total radiated power from the LHD plasma is measured with a wide-angle resistive bolometer,¹⁷ which is installed at the same Port 3-O as the TESPEL injector. The effective temporal resolution of this bolometer is 5–10 ms.

III. RESULTS OF PROOF-OF-PRINCIPLE EXPERIMENT

In the proof-of-principle experiment, a high electron density (about $5 \times 10^{19} \text{ m}^{-3}$ as a line-averaged electron density) was set for the target plasma because it is expected that there is a significant difference between the behaviors of low- and mid-Z impurities in such high-density plasmas. In previous work on LHD, impurity accumulation has been observed in plasmas with such a high electron density.¹⁸ The impurity accumulation observed in LHD is mainly attributed to a larger inward convective flux driven by a negative radial electric field, compared to an outward diffusion flux. The convective term driven by the radial electric field in the impurity particle flux formula has a positive Z dependence.¹⁹

In the first test of the proof-of-principle experiment, a single Li_2TiO_3 -TESPEL was used. Figure 2 shows typical waveforms of the plasma in this first test. In LHD, the charge exchange (CX) line intensity is derived from the difference of the line intensity between a neutral beam-on time and a neutral beam-off time. For this purpose, NBI No. 4 is used as a probe beam for CXS and is modulated with 90% duty cycle (180 ms on and 20 ms off). In order to avoid the change in total injected NBI power as much as possible, NBI No. 5 is modulated with 10% duty cycle (20 ms on and 180 ms off) and is operated out of phase with NBI No. 4. The single Li_2TiO_3 -TESPEL was injected at the time of about 4.14 s during heating with NBI No. 2, NBI No. 3, and NBI No. 4. The Li_2TiO_3 -TESPEL injection produced a very sharp spike in the plasma radiation. This is because the wide-angle resistive bolometer can detect directly the ablation emission from the TESPEL. After its sharp peak, the plasma radiation

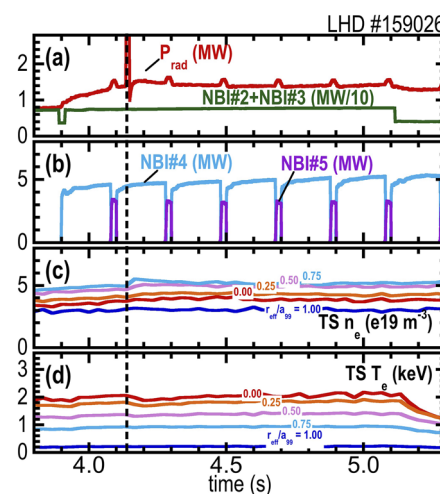


FIG. 2. Time traces of the discharge for the first test: (a) plasma radiation and port-through power of NBI No. 2 + NBI No. 3, (b) port-through power of NBI No. 4 and NBI No. 5 (c) electron density, and (d) electron density at different normalized minor radii, which are estimated from Thomson scattering data.

returned almost to the pre-injection level. As shown in Fig. 2(c), a slight increase in electron density was obtained at the edge ($r_{\text{eff}}/a_{99} > 0.5$). Here, r_{eff} is an averaged minor radius on a magnetic flux surface and a_{99} is an effective minor radius in which 99% of the plasma kinetic energy is confined. As can be seen from Fig. 3(a), the peak location of the density increases because the TESPEL injection was found to be at around $R \sim 4.37$ m ($r_{\text{eff}}/a_{99} \sim 0.85$). A slight decrease in core electron temperature was also obtained due to the cold pulse propagation²⁰ induced by the TESPEL injection. These results indicate that the single Li_2TiO_3 -TESPEL injection into the plasma has little impact on the plasma conditions, i.e., the single Li_2TiO_3 -TESPEL injection does not lead to plasma termination. In the case of single Li_2TiO_3 -TESPEL, the intensities of CX Li III and CX O VIII spectral lines obtained were marginal levels, even immediately after the TESPEL injection. At $R \sim 4.37$ m, the peak location of the density increases, the CX Li III intensity at $t = 4.15$ s was slightly higher than the zero level, whereas the CX O VIII intensity at $t = 4.15$ s is still almost zero. These results were considered to be due to an insufficient amount of the Li_2TiO_3 tracer. However, line emissions, such as Ti XX (Li-like, $\lambda = 25.93$ nm, $1s^22s^2S_{1/2}-1s^22p^2P_{3/2}$), from the highly charged Ti ions were clearly observed.

In the second test of the proof-of-principle experiment, we performed a double Li_2TiO_3 -TESPEL injection in order to increase the amount of Li_2TiO_3 deposited by the TESPEL injection. The almost simultaneous injection of two TESPELs into the plasmas can be performed because each small storage chamber (its depth is 5 mm) in the TESPEL magazine disk can hold more than one TESPEL and each small storage chamber can be set very precisely at the injection axis by using a remote-controlled motor.²¹ Figure 4 shows typical

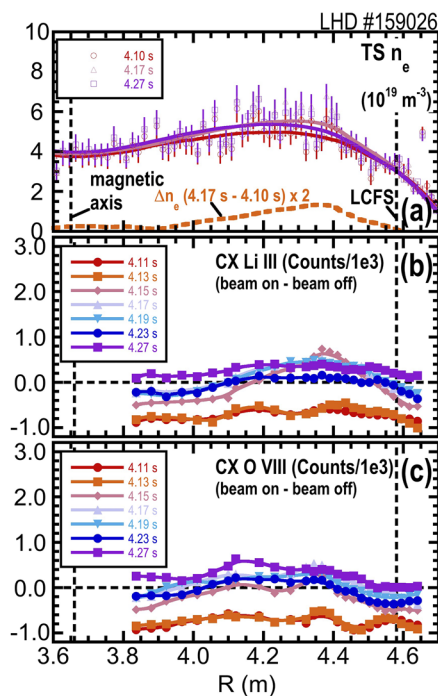


FIG. 3. Radial profiles of (a) electron density, (b) CX Li III intensity, and (c) CX O VIII intensity at different times for the first test.

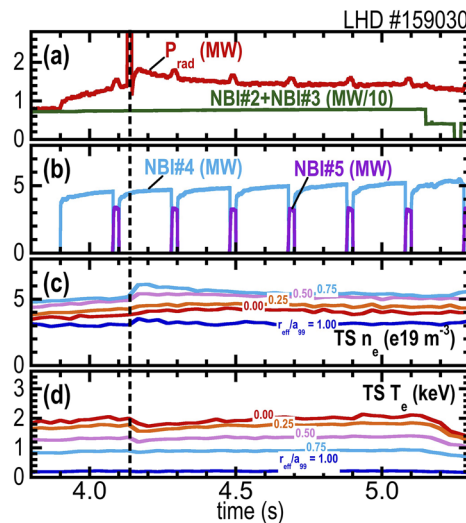


FIG. 4. Time traces of the discharge for the second test: (a) plasma radiation and port-through power of NBI No. 2 + NBI No. 3, (b) port-through power of NBI No. 4 and NBI No. 5, (c) electron density, and (d) electron temperature at different normalized minor radii, which are estimated from Thomson scattering data.

time traces of the discharge in the second test. The two Li_2TiO_3 -TESPELs were injected almost simultaneously at the time of ~ 4.13 s. As is the case with the single Li_2TiO_3 -TESPEL injection, the plasma radiation showed a sharp peak due to the TESPEL injection. After the sharp peak, the plasma radiation did not return to the pre-injection level, but gradually decreased. It is considered that this could be an effect of the impurities injected. As shown in Fig. 4(c), a slight increase in electron density was obtained in a wider region ($r_{\text{eff}}/a_{99} > 0.25$). However, as indicated by Fig. 5(a), the peak location of the density increment by the TESPEL injection was found to be almost at the same position, about $R \sim 4.34$ m ($r_{\text{eff}}/a_{99} \sim 0.84$), as the single TESPEL case. Thus, this fact suggests that the penetration depth of the TESPELs was almost the same as the single TESPEL case. In this case also, a cold pulse propagation induced by this double-TESPEL injection was observed. In addition, this double Li_2TiO_3 -TESPEL injection into the plasma has a larger impact on the plasma conditions, but nonetheless it still does not lead to plasma termination. By using the double Li_2TiO_3 -TESPEL injection, the intensities of CX Li III and CX O VIII obtained after the TESPEL injection reached significant levels. As can be easily recognized from Figs. 5(b) and 5(c), the spatiotemporal evolution of CX Li III and CX O VIII intensities above the net zero level was clearly observed. The radial profile of the CX Li III intensity ($t = 4.13$ s) right after the TESPEL injection is found to be already spread to some extent. This is because, the fully ionized Li ions were already transported during 20 ms, which is the temporal resolution of CXS system. The local maximum of the CX Li III intensity is found to exist at around $R = 4.35$ m. As shown in Fig. 5(a), this position seems to correspond to the local maximum position of the increase in electron density after the Li_2TiO_3 -TESPEL injection. The peak position of the CX Li III intensity seems to move inward to some extent until finally the CX Li III intensity can no longer be observed. The radial profiles of the observed CX O VIII intensity showed broader profiles when

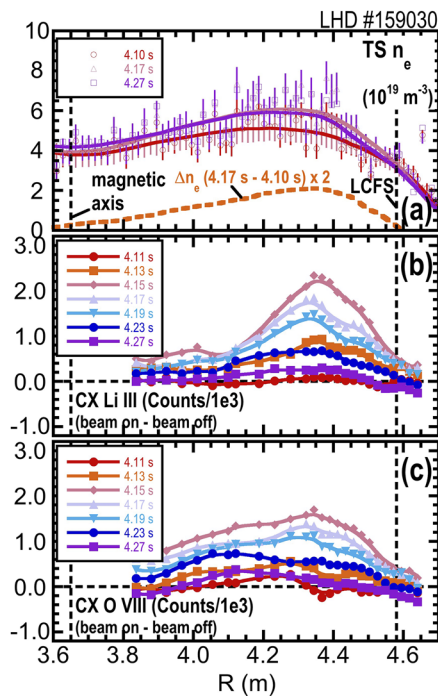


FIG. 5. Radial profiles of (a) electron density, (b) CX Li III intensity, and (c) CX O VIII intensity at different times for the second test.

compared with the radial profile of the CX Li III intensity. However, the local maximum of the CX O VIII intensity is found to be at almost the same position as the CX Li III intensity, $R = 4.35$ m. This result indicates that the dominant deposition location of the Li_2TiO_3 tracer would exist at $R \sim 4.35$ m ($r_{\text{eff}}/a_{99} \sim 0.84$). Therefore, the total penetration depth of the double TESPELs should be slightly beyond the $r_{\text{eff}}/a_{99} = 0.84$ location, because the tracer impurity in the TESPEL will be exposed to the plasma at the final phase of the entire TESPEL ablation. The penetration depth r_{eff}/a_{99} of ~ 0.84 is quite similar to the typical penetration depth of previous TESPELs having the pure element tracers,²² and still much deeper than that of a laser blow-off method.²³ The peak location of the CX O VIII intensity seems to move more inward compared with the CX Li III intensity. The difference in the spatiotemporal behavior between CX Li III and CX O VIII may reflect the differences (1) in the transport characteristics of fully ionized Li and O ions and (2) in the abundance distribution of those ions in the plasma.

Figure 6 shows the temporal evolutions of the intensities of CX Li III, CX O VIII, and Ti XX obtained during the first and second tests. Here, for the purpose of comparison, the CX Li III and CX O VIII intensities are integrated over all the spatial channels along the major radius. Due to its integration effect, the integrated intensity can show a positive value even before the Li_2TiO_3 -TESPEL injection. The average level of the integrated intensity during the time period before the Li_2TiO_3 -TESPEL injection is estimated as the noise level. As can be easily recognized from Figs. 6(a) and 6(b), the spatially integrated intensities of CX Li III and CX O VIII lines in the first test are below the noise level. However, the spatially integrated intensities of the same CX Li III and CX O VIII

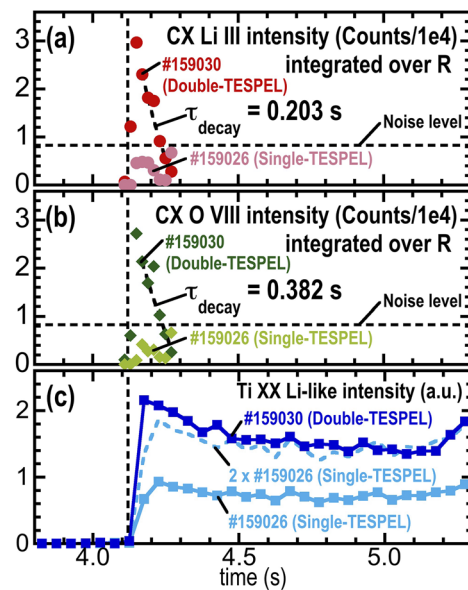


FIG. 6. Temporal evolutions of intensities of (a) CX Li III line, (b) CX O VIII line, and (c) Ti XX line obtained in the first and second tests. The vertical dashed line indicates the TESPEL injection time. For the purpose of comparison, the intensities of CX Li III and CX O VIII are integrated over the major radius.

lines in the second test clearly show significant temporal evolutions, i.e., they decayed rapidly. The decay times of these spatially integrated CX Li III and CX O VIII intensities, which are evaluated from the fitting of an exponential decay, are evaluated to be 0.203 and 0.382 s, respectively. On the other hand, as can be seen from Fig. 6(c), the intensities of Ti XX in both tests were kept at a high level up for around 5.2 s, where the core electron temperature was decreased due to the decrease in the total port-through power of NBI. These facts indicate that the accumulation of Ti impurity occurred in both tests. From a comparison between the Ti XX intensity with the double TESPEL and the same line intensity with the single TESPEL, it is found that the double-TESPEL injection delivered successfully twice the amount of Li_2TiO_3 compared to the single TESPEL into the plasma. This is also confirmed from the particle inventory in the plasma. The expected electron density increase by the single and double TESPELs is estimated to be $4.3 \times 10^{18} \text{ m}^{-3}$ ($4.2 \times 10^{18} \text{ m}^{-3}$ from the shell and $9.2 \times 10^{16} \text{ m}^{-3}$ from the Li_2TiO_3 tracer) and $8.6 \times 10^{18} \text{ m}^{-3}$ ($8.4 \times 10^{18} \text{ m}^{-3}$ from the shell and $1.8 \times 10^{17} \text{ m}^{-3}$ from the Li_2TiO_3 tracer), respectively. Here, the filling rate of the Li_2TiO_3 tracer into the TESPEL shell is assumed to be 20%. As can be seen, the dominant electron supplier is the TESPEL shell. The electron density increments by the single and double-TESPEL injections, which are estimated from the line-averaged electron density measurement, were estimated to be $2.88 \times 10^{18} \text{ m}^{-3}$ ($\times 2 = 5.76 \times 10^{18} \text{ m}^{-3}$) and $6.05 \times 10^{18} \text{ m}^{-3}$, respectively. In this case, about 70% of the particles in the TESPEL are considered to be deposited in the plasma. Considering measurement uncertainties, the discrepancy in the electron density increments between the single TESPEL and the double single TESPEL would be within the uncertainty. The difference in the decay characteristics obtained between CX Li III, CX O VIII, and Ti XX indicates clearly

the existence of Z dependence in LHD. Therefore, the second test of the proof-of-principle experiment demonstrated clearly the applicability of another new multi-tracer technique using the inorganic compound.

IV. DISCUSSION

In this proof-of-principle experiment, the multi-TESPEL injection method has been implemented. However, in an actual experiment for the precise Z dependence study of impurity transport, such a double-TESPEL injection would not be acceptable because almost the simultaneous injection of two TESPELs in the same injection line could make it very difficult to determine which signal is from which TESPEL in the TESPEL velocity measurement, i.e., to identify the deposition location and width of the impurity tracers from each TESPEL. Therefore, the improvement of the TESPEL payload capacity is urgently needed. The thin-shell-type TESPEL is more favorable for this purpose. Currently, we have the polystyrene shell with an outer diameter of 700 μm and an inner core diameter of 550 μm (the shell thickness of 75 μm) and the polystyrene shell with an outer diameter of 600 μm and an inner core diameter of 440 μm (the shell thickness of 80 μm). From past experience with such polystyrene shells, and to be on the safe side, the polystyrene shell with an outer diameter of 900 μm and an inner core diameter of 660 μm (the shell thickness being 120 μm) is currently under development. Compared with the thick-shell-type TESPEL²⁴ having the outer diameter of 900 μm and the inner core diameter of 300 μm , i.e., a shell thickness of 300 μm (used in the proof-of-principle experiment), the TESPEL payload capacity will increase approximately tenfold. Therefore, based on the results of the second test of the proof-of-principle experiment, a single TESPEL containing a sufficient amount of the inorganic compound impurity tracer will be applicable in the very near future.

In order to complete the Z dependence study of impurity transport in magnetically confined high-temperature plasmas, various inorganic compound impurity tracers are needed. In high-density LHD NBI-heated plasmas, the accumulation of Ti ($Z = 22$) impurity has been frequently observed. At the same time, the second test of the proof-of-principle experiment indicates that Li ($Z = 3$) and O ($Z = 8$) were not accumulated in such high-density LHD NBI-heated plasmas. Therefore, a change in impurity transport characteristics from “exhaust” to “accumulation,” in other words, a sign of convective flux from “outward” to “inward” in LHD, should occur in some impurities between $Z = 8$ and $Z = 22$. Currently, calcium aluminate (CaAl_2O_4) and silicon hexaboride (SiB_6), in addition to lithium titanate (Li_2TiO_3), are considered as possible candidates in such a precise Z dependence study of impurity transport in LHD.

V. SUMMARY

A new multi-tracer technique in the Tracer-Encapsulated Solid Pellet (TESPEL) method has been developed for studying simultaneously the behaviors of low- and mid/high-Z impurities in magnetically confined high-temperature plasmas. In this new technique, an inorganic compound (for example, lithium titanate, Li_2TiO_3) is proposed to be used as a tracer embedded in the core of the TESPEL, instead of pure elements. For the proof-of-principle

experiment, a two-wavelength spectrometer was used for the simultaneous measurement of CX lines of Li and O. In order to overcome limitations of the payload capacity of the currently available TESPEL shells, the synchro-multiple TESPEL injection method was applied. Consequently, the behaviors of low-Z impurity (Li and O) and mid-Z impurity (Ti) were successfully observed with CXS and the EUV/VUV spectrometer, respectively. In the high-density LHD NBI-heated plasma, decay times of Li and O ions are found to be much shorter than the decay time of Ti ions. This result indicates clearly the existence of Z dependence of impurity transport in LHD. Therefore, the proof-of-principle experiment demonstrated clearly the applicability of the new multi-tracer technique using the inorganic compound. As future work, a variety of single TESPELs containing different compound impurity tracers will be developed to promote the precise study of Z dependence of impurity transport in LHD.

ACKNOWLEDGMENTS

We would like to thank the LHD experiment group and the technical staff of LHD for their effort to support the experiment in LHD, as well as Dr. Kieran J. McCarthy (CIEMAT) for his helpful suggestions and proofreading. This work was supported by a Grant-in-Aid for Young Scientists from the Toray Scientific Foundation, by JSPS KAKENHI (Grant No. JP19H01881), and by a budgetary Grant-in-Aid (Grant Nos. ULHH007 and ULHH012) of the National Institute for Fusion Science.

DATA AVAILABILITY

The data that support the findings of this study are available from the corresponding author upon reasonable request.

REFERENCES

- ¹K. Ida *et al.*, *Phys. Rev. Lett.* **58**, 116 (1987).
- ²R. Dux *et al.*, *Nucl. Fusion* **39**, 1509 (1999).
- ³C. Giroud *et al.*, *Nucl. Fusion* **47**, 313 (2007).
- ⁴R. Guirlet *et al.*, *Nucl. Fusion* **49**, 055007 (2009).
- ⁵B. A. Grierson *et al.*, *Phys. Plasmas* **22**, 055901 (2015).
- ⁶S. Sudo *et al.*, *Plasma Phys. Controlled Fusion* **55**, 095014 (2013).
- ⁷M. Gaja and M. Z. Tokar, *Plasma Phys. Controlled Fusion* **59**, 025001 (2017).
- ⁸B. Zurro *et al.*, *Plasma Phys. Controlled Fusion* **56**, 124007 (2014).
- ⁹A. Langenberg *et al.*, *Phys. Plasmas* **27**, 052510 (2020).
- ¹⁰S. S. Henderson *et al.*, *Plasma Phys. Controlled Fusion* **57**, 095001 (2015).
- ¹¹S. Sudo, *J. Plasma Fusion Res.* **69**, 1349 (1993).
- ¹²S. Sudo *et al.*, *Nucl. Fusion* **52**, 063012 (2012).
- ¹³N. Tamura *et al.*, *Rev. Sci. Instrum.* **87**, 11D615 (2016).
- ¹⁴K. Ida *et al.*, *Rev. Sci. Instrum.* **86**, 123514 (2015).
- ¹⁵J. L. Schwob *et al.*, *Rev. Sci. Instrum.* **58**, 1601 (1987).
- ¹⁶K. Narihara *et al.*, *Rev. Sci. Instrum.* **72**, 1122 (2001).
- ¹⁷B. J. Peterson *et al.*, *Plasma Phys. Controlled Fusion* **45**, 1167 (2003).
- ¹⁸N. Tamura *et al.*, *Phys. Plasmas* **24**, 056118 (2017).
- ¹⁹V. Tribaldos, *Phys. Plasmas* **8**, 1229 (2001).
- ²⁰S. Inagaki *et al.*, *Nucl. Fusion* **46**, 133 (2006).
- ²¹S. Sudo and N. Tamura, *Rev. Sci. Instrum.* **83**, 023503 (2013).
- ²²N. Tamura *et al.*, *Plasma Phys. Controlled Fusion* **58**, 114003 (2016).
- ²³G. Kocsis *et al.*, *IEEE Trans. Plasma Sci.* **24**, 1120 (1996).
- ²⁴N. Tamura *et al.*, *Plasma Fusion Res.* **10**, 1402056 (2015).